Обзор ArXiv: astro-ph, 16-19 мая 2017 года

От Сильченко О.К.

Astro-ph: 1705.04692

Galactic Outflows, Star Formation Histories, and Timescales in Starburst Dwarf Galaxies from STARBIRDS

Kristen. B. W. McQuinn,[1,2⋆] Evan D. Skillman,[2] Taryn N. Heilman,[2] Noah P. Mitchell,[2,3] Tyler Kelley[2,4]

[1] *The University of Texas at Austin, Department of Astronomy, 2515 Speedway, Stop C1400, Austin, Texas 78712-1205*

[2] *Minnesota Institute for Astrophysics, School of Physics and Astronomy, 116 Church Street, S.E., University of Minnesota, Minneapolis, MN 55455*

[3] *Department of Physics and the James Franck Institute, The University of Chicago, 929 East 57th Street, Chicago, Illinois 60637*

[4] *Department of Physics and Astronomy, University of California, Irvine, 4129H Frederick Reines Hall, Irvine CA 92697-4575*

16 May 2017

ABSTRACT

Winds are predicted to be ubiquitous in low-mass, actively star-forming galaxies. Observationally, winds have been detected in relatively few local dwarf galaxies, with even fewer constraints placed on their timescales. Here, we compare galactic outflows traced by diffuse, soft X-ray emission from *Chandra Space Telescope* archival observations to the star formation histories derived from Hubble Space Telescope imaging of the resolved stellar populations in six starburst dwarfs. We constrain the longevity of a wind to be of order 25 Myr based on galaxies whose starburst activity has already declined, although a larger sample is needed to confirm this result. Compared

Выборка и рентгеновские данные Chandra

Galaxy	RA (J2000)	Dec (J2000)	M_B (mag)	Dist. (Mpc)	A_V (mag)	12+log(O/H)	Principal Investigator	Obs. No.	Exp. Time (ksec)
DDO 165	13:06:24.85	+67:42:25.0	12.92	4.81	0.07	7.80	Jenkins	9537	13.7
								10868	10.7
NGC 625	01:35:04.63	−41:26:10.3	11.65	4.21	0.05	8.10	Skillman	4746	61.1
NGC 1569	04:30:49.06	+64:50:52.60	11.72	3.36	1.9	8.19	Martin	782	98.0
							Zezas	4745	10.2
NGC 4214	12:15:39.17	+36:19:36.8	10.21	2.95	0.06	8.38	Zezas	4743	27.6
								5197	29.0
							Heckman	2030	26.8
NGC 4449	12:28:11.10	+44:05:37.07	9.50	4.31	0.05	8.32	Long	10125	15.1
								10875	60.2
							Heckman	2031	26.9
NGC 5253	13:39:55.96	−31:38:24.38	10.80	3.56	0.15	8.10	Zezas	7153	69.1
								7154	67.5
							Heckman	2032	57.4

Истории звездообразования по подсчетам отдельных звезд

Galaxy	M_* $\times 10^6$ ($M_\odot$)	sSFR $\times 10^{-10}$ (yr^{-1})	Peak Burst SFR $\times 10^{-3}$ ($M_\odot$ yr^{-1})	Time since Burst Peak (Myr)	Burst Duration (Myr)	Concentration of Stars (%)
DDO 165	190	4	80±5	65	$> 1300 \pm 500$	45
NGC 625	260	2	40±2	450 (65)	450 ± 50	90
NGC 1569	700	2	130±40	65	$> 450 \pm 50$	85
NGC 4214	280	5	130±40	450	$> 810 \pm 190$	...
NGC 4449	2100	5	970±70	7.5	$> 450 \pm 50$	72
NGC 5253	150	6	970±70	450	$> 450 \pm 50$	87

Table 2. Star Formation Properties: Measurements of star formation properties for the galaxies in our sample from (McQuinn et al. 2010b). Col. 2. The cumulative stellar mass in the *HST* field of view based on the total stellar mass formed over the lifetime of the galaxy and assuming a recycling fraction of 30% (Kennicutt et al. 1994). Col. 3. Average SFR over the past 10 Myr normalized by the cumulative stellar mass. Col. 4. Peak (not average) SFR of the burst. Col.5 Time since the peak SFR of the burst. For post-starburst galaxy NGC 625, the second value represents the time since the burst ended. Col. 6. Burst duration. Col. 7 Concentration of the recent star formation activity relative to the stellar disc calculated from the spatial distribution of BHeB to RGB stars (i.e., 1 - BHeB extent/RGB extent; McQuinn et al. 2012). For NGC 4214, the areal coverage of the *HST* imaging was insufficient to compare the spatial distribution of the BHeB and RGB stars.

Типичные рентгеновские морфологии

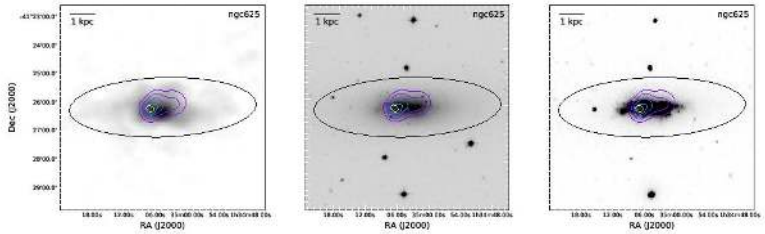

Figure 2. NGC 625. *Left:* 21 cm neutral hydrogen emission map. *Middle:* DSS R-band optical image. *Right:* GALEX NUV image. Each image is overlaid with contours of soft X-ray emission corresponding to 2, 4, 8, 16, 32, and 64 σ. The black ellipse represent the main optical disk of the galaxy measured by the 25 m_B arcsec^{-2} isophote. Extended diffuse X-ray emission is detected around the star forming disc of the galaxy out to the edges of the gaseous disc along the minor axis.

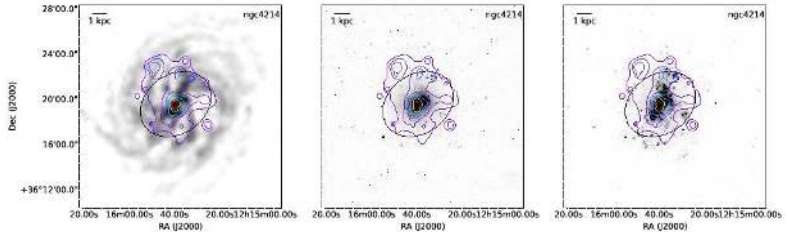

Figure 4. NGC 4214. *Left:* 21 cm neutral hydrogen emission map. *Middle:* DSS R-band optical image. *Right:* GALEX NUV image), each overlaid with contours of soft X-ray emission corresponding to 2, 4, 8, 16, 32, and 64 σ. The black ellipse represent the main optical disk of the galaxy measured by the 25 m_B arcsec^{-2} isophote. The diffuse soft X-ray emission is extended in a number of regions outside the star forming disc and coincides with a low density cavity in the HI to the west.

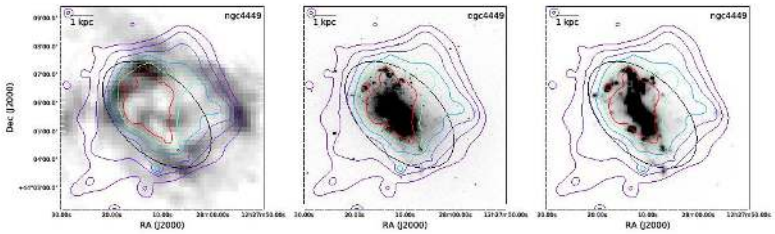

Figure 5. NGC 4449. *Left:* 21 cm neutral hydrogen emission map. *Middle:* DSS R-band optical image. *Right:* GALEX NUV image), each overlaid with contours of soft X-ray emission corresponding to 2, 4, 8, 16, 32, and 64 σ. The black ellipse represent the main optical disk of the galaxy measured by the 25 m_B arcsec^{-2} isophote. The diffuse soft X-ray is widely extended along the minor axis of the galaxy with the strongest evidence of an outflow in the southeast.

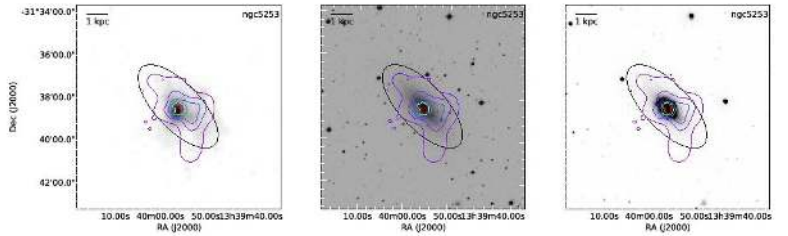

Figure 6. NGC 5253. *Left:* 21 cm neutral hydrogen emission map. *Middle:* DSS R-band optical image. *Right:* GALEX NUV image. Each image is overlaid with contours of soft X-ray emission corresponding to 2, 4, 8, 16, 32, and 64 σ. The black ellipse represent the main optical disk of the galaxy measured by the 25 m_B arcsec^{-2} isophote. Diffuse soft X-ray surrounds the central region and extends past the HI disc in the south and, to a lesser extent, in the west.

Крайние случаи:

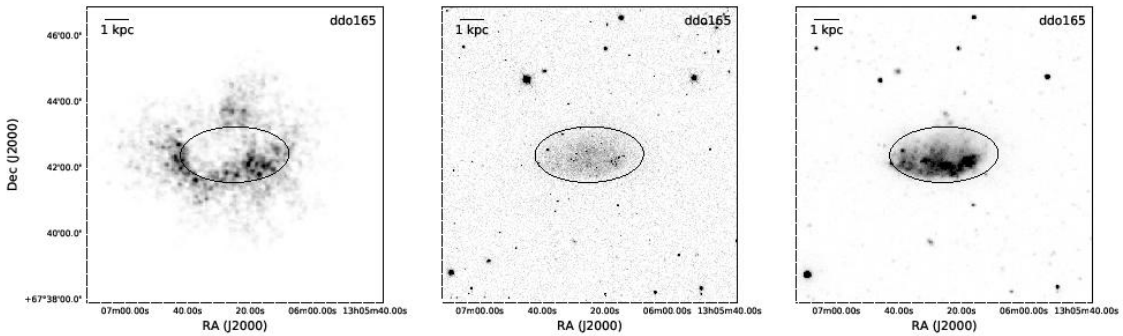

Figure 1. DDO 165. *Left:* 21 cm neutral hydrogen emission map. *Middle:* DSS R-band optical image. *Right:* GALEX NUV image. The black ellipse represent the main optical disk of the galaxy measured by the 25 m_B arcsec^{-2} isophote. No diffuse X-ray emission was detected.

DDO 165 – нет никакого ветра

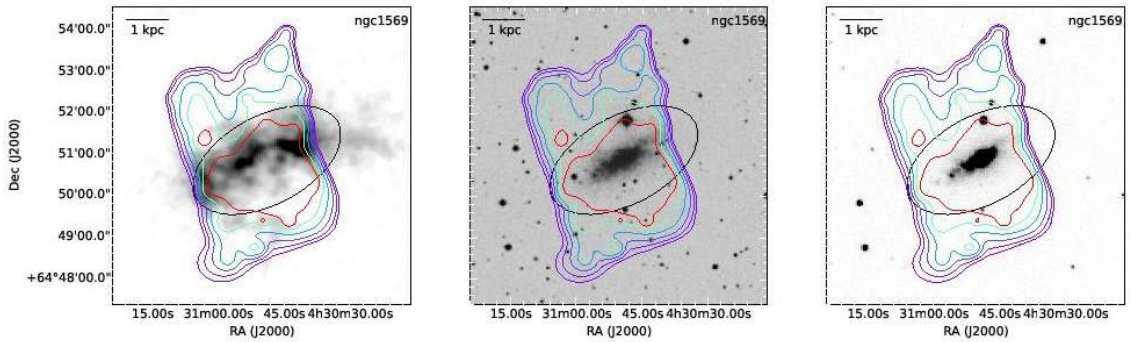

Figure 3. NGC 1569. *Left:* 21 cm neutral hydrogen emission map. *Middle:* DSS R-band optical image. *Right:* GALEX NUV image. Each image is overlaid with contours of soft X-ray emission corresponding to 2, 4, 8, 16, 32, and 64 σ. The black ellipse represent the main optical disk of the galaxy measured by the 25 m_B arcsec^{-2} isophote. Diffuse soft X-ray emission traces a large-scale outflow along the minor axis of the galaxy.

NGC 1569 – мощно «дует» по всему диску

Оценка длительности фазы ветра:

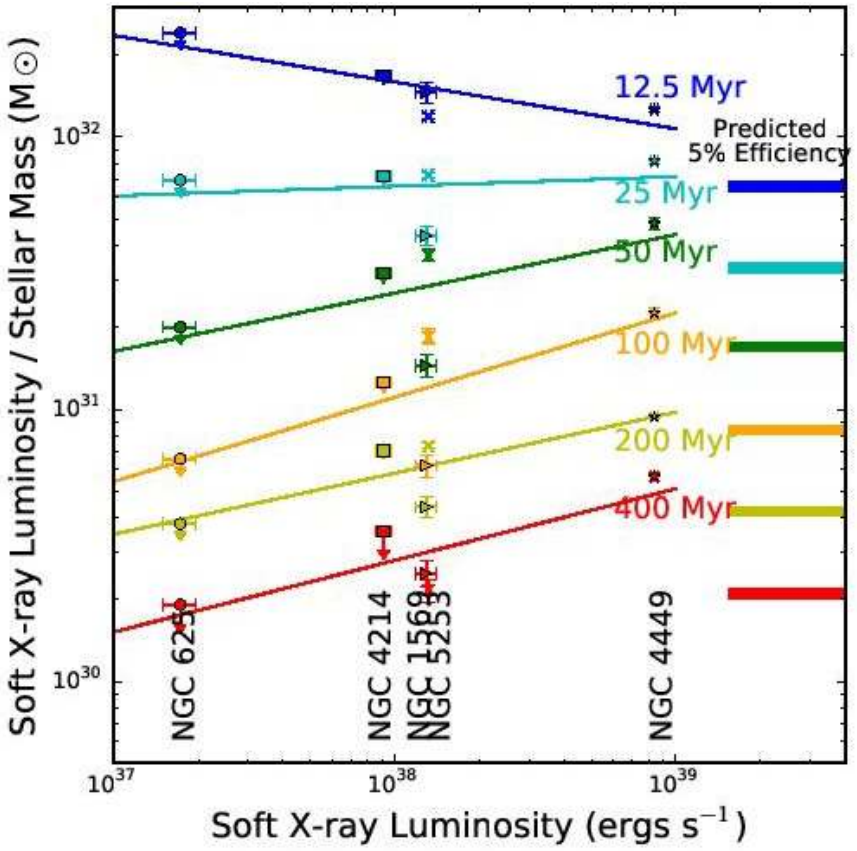

Figure 7. Soft X-ray luminosity compared with the soft X-ray luminosity / stellar mass formed in different time periods from the SFHs for the 5 galaxies with detected soft X-ray emission.

Результаты и выводы

Comparing the X-ray luminosities to the mechanical energy injected by stellar feedback over different timescales, we find the diffuse soft X-ray emission accounts for $15-31\%$ of the energy from star formation deposited over short 10 Myr timescales (with upper limits from two systems of 56% and 69%), but represents $< 1\%$ of the energy from the full starburst events based on modelling from the SFHs. These ratios bracket the starburst event and indicate that the outflows have been sustained for a significant fraction of the burst duration. Such temporally extended outflows suggest that expelled material may reach farther distances before cooling, increasing the amount of material than will reach the CGM or IGM and potentially lowering the recycling fraction of gas back to the ISM. Over the wind timescale of 25 Myr, the average wind efficiency is 16%. This can be compared with $< 10\%$ predicted from numerical simulations and 5% from studies of spiral galaxies.

Astro-ph: 1705.05733

Arm and interarm abundance gradients in CALIFA spiral galaxies

L. Sánchez-Menguiano[1,2], S. F. Sánchez[3], I. Pérez[2,4], V. P. Debattista[5], T. Ruiz-Lara[2,4,6,7], E. Florido[2,4], O. Cavichia[8], L. Galbany[9], R. A. Marino[10], D. Mast[11,12], P. Sánchez-Blázquez[13], J. Méndez-Abreu[6,7,14], A. de Lorenzo-Cáceres[3], C. Catalán-Torrecilla[15], M. Cano-Díaz[3], I. Márquez[1], D. H. McIntosh[16], Y. Ascasibar[17,18], R. García-Benito[1], R. M. Gónzalez Delgado[1], C. Kehrig[1], Á. R. López-Sánchez[19,20], M. Mollá[21], J. Bland-Hawthorn[22], C. J. Walcher[23], and L. Costantin[24]

Пример анализа: выделялись рукава шириной 4” и оценивался градиент металличности отдельно в рукавах и в межрукавном пространстве

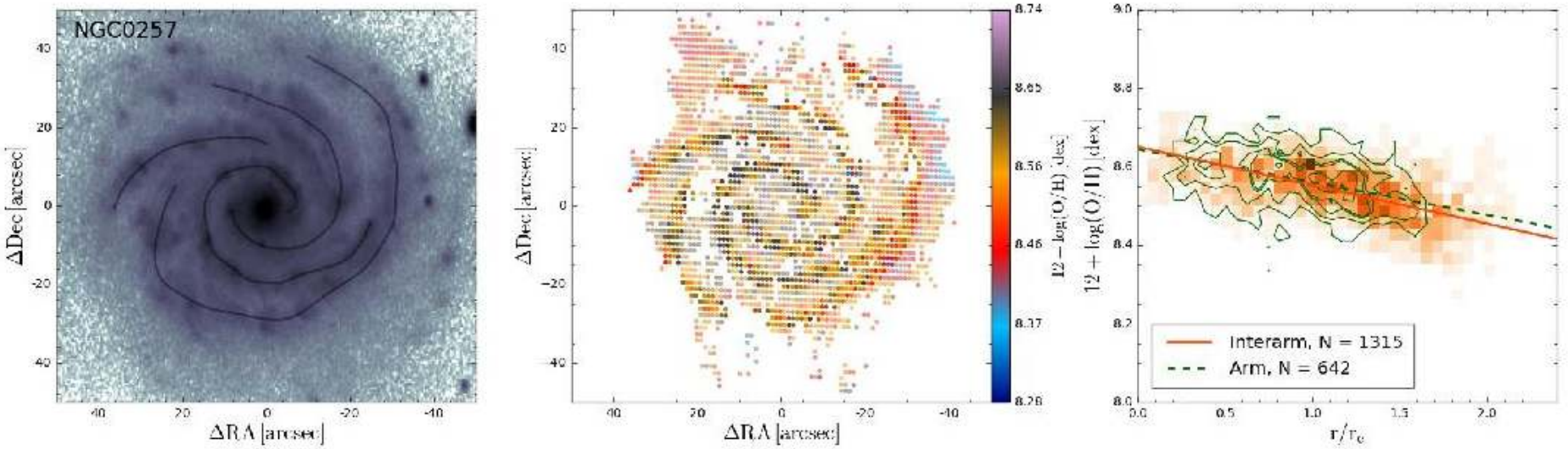

Fig. 3. NGC0257. *Left panel:* Outline of the spiral arms on the deprojected SDSS *g*-band map. *Middle panel:* Colour map of the oxygen abundance distribution of the spiral arms (opaque dots) and the interarm region (transparent dots). *Right panel:* Radial density distribution in the oxygen abundance-galactocentric distance space of the spaxels located in the spiral arms (green contours) and those associated with the interarm region (orange colour map). The outermost contour encircles 100% of the total number of spaxels, decreasing by 20% in each consecutive contour. The lines represent the error-weighted linear fit derived for the arm (green dashed line) and interarm (orange solid line) distributions. The inset indicates the number of spaxels of each distribution that contribute to the derivation of the gradient, i.e. located within the radial range 0.5-2.0 r_e.

Результаты

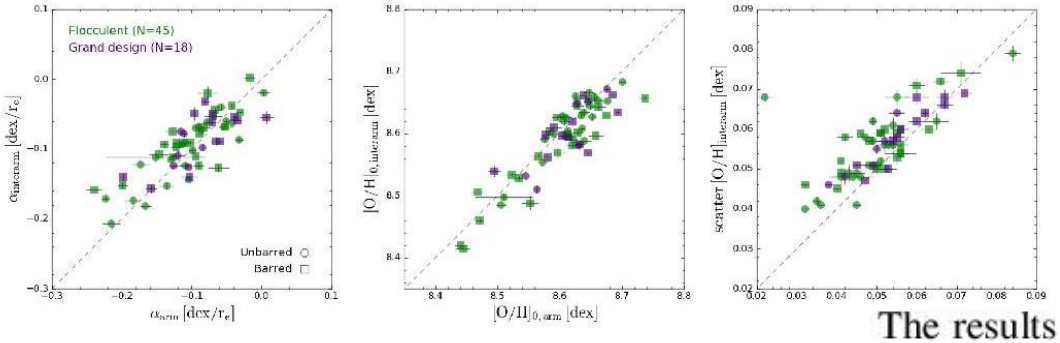

Grand-design vs flocculent

The results of our analysis show that subtle differences exist between the arm and interarm radial abundance distribution. After performing Student's *t*-tests we conclude that only the differences found in flocculent and barred galaxies are statistically significant. On average, we find that the ionised gas in the interarm regions of these subgroups of galaxies presents a shallower gradient with a lower zero-point value and a larger dispersion in the oxygen abundances. Furthermore, we find that for flocculent galaxies this dispersion correlates with the angular distance to the spiral arms: the farthest spaxels present the larger scatter. Grand design galaxies, on the other hand, do not seem to present any trend in the dispersion with the distance to the arms. The

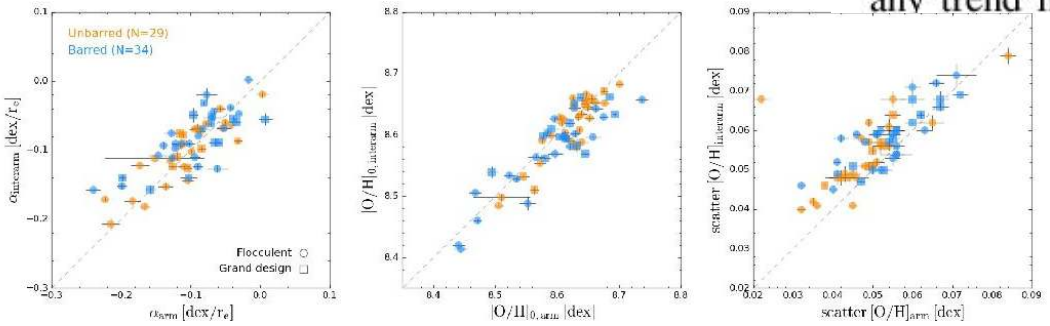

Barred vs unbarred

Astro-ph: 1705.05892

Warm-hot gas in X-ray bright galaxy clusters and the H I-deficient circumgalactic medium in dense environments

Joseph N. Burchett[1†], Todd M. Tripp[1], Q. Daniel Wang[1], Christopher N.A. Willmer[2], David V. Bowen[3], Edward B. Jenkins[3]

[1] *University of Massachusetts - Amherst*
[2] *Steward Observatory, University of Arizona*
[3] *Princeton University Observatory*
[†] *Corresponding author: jburchet@astro.umass.edu*

18 May 2017

ABSTRACT

We analyze the intracluster medium (ICM) and circumgalactic medium (CGM) in 7 X-ray detected galaxy clusters using spectra of background QSOs from the Hubble Space Telescope (HST) Cosmic Origins Spectrograph (COS) and Space Telescope Imaging Spectrograph (STIS), optical spectroscopy of the cluster galaxies from MMT/Hectospec and the Sloan Digital Sky Survey (SDSS), and X-ray imaging/spectroscopy from XMM-Newton and Chandra. First, the optical spectroscopy reveals many galaxies at small impact parameters (< 300 kpc) to the QSO sightlines and within ~ 1000 km s^{-1} of the cluster redshifts; we report a very low covering fraction of H I absorption in the CGM of these cluster galaxies, $f_c = 18^{+14}_{-9}\%$, to

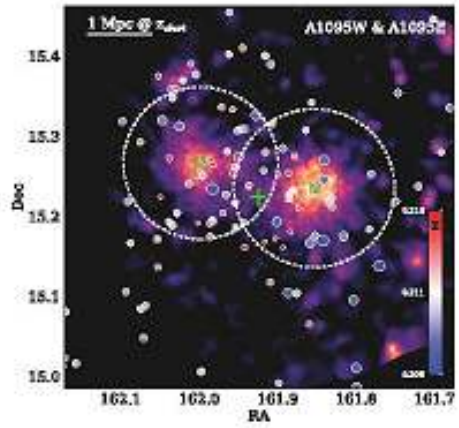
1 Mpc @ z_{clust}
A1095W & A1095E
15.4
15.3
15.2
15.1
15.0
Dec
163.1
163.0
161.9
161.8
161.7
RA

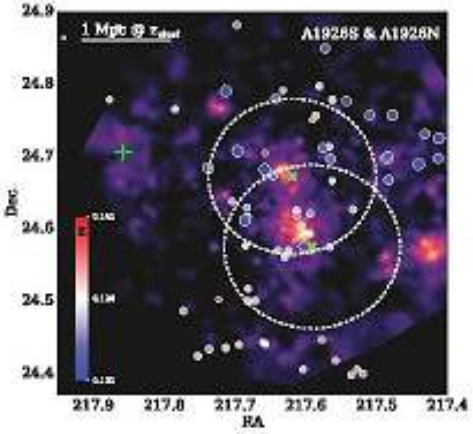
1 Mpc @ z_{clust}
A1926S & A1926N
24.9
24.8
24.7
24.6
24.5
24.4
Dec
217.9
217.8
217.7
217.6
217.5
217.4
RA

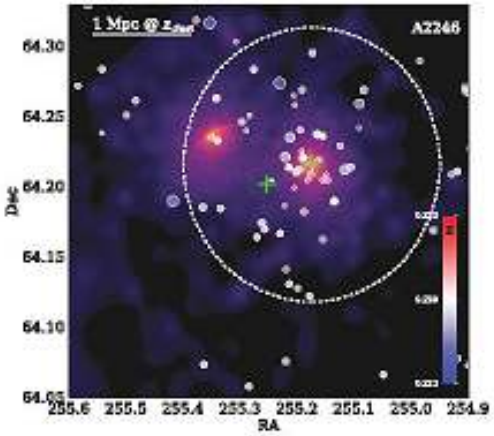
1 Mpc @ z_{clust}
A2246
64.30
64.25
64.20
64.15
64.10
64.05
Dec
255.6
255.5
255.4
255.3
255.2
255.1
255.0
254.9
RA

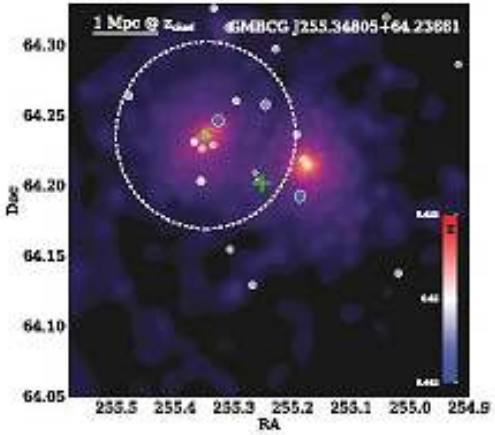
1 Mpc @ z_{clust}
GMBCG J255.34805+64.23681
64.30
64.25
64.20
64.15
64.10
64.05
Dec
255.5
255.4
255.3
255.2
255.1
255.0
254.9
RA

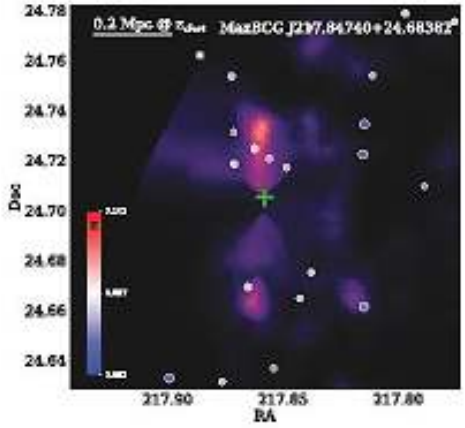
0.2 Mpc @ z_{clust}
MaxBCG J217.84740+24.68382
24.78
24.76
24.74
24.72
24.70
24.68
24.66
24.64
Dec
217.90
217.85
217.80
RA

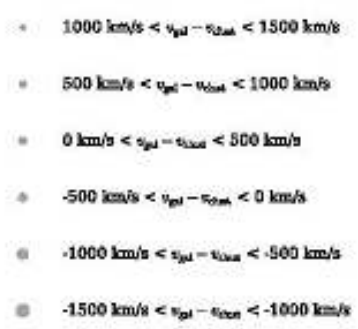
1000 km/s < $v_{gal} - v_{clust}$ < 1500 km/s
500 km/s < $v_{gal} - v_{clust}$ < 1000 km/s
0 km/s < $v_{gal} - v_{clust}$ < 500 km/s
-500 km/s < $v_{gal} - v_{clust}$ < 0 km/s
-1000 km/s < $v_{gal} - v_{clust}$ < -500 km/s
-1500 km/s < $v_{gal} - v_{clust}$ < -1000 km/s

Выборки скоплений и квазаров

Cluster	z_c [a]	log M_{200} [log $M_\odot$]	r_{200} [kpc]	ρ_{cl} [b] [kpc]	QSO
Abell 1095E	0.213	14.4	1240	865	SDSS J104741.75+151332.2
Abell 1095W	0.210	14.4	1190	1046	
Abell 1926S	0.136	14.1	990	2411	2MASS J1431258+244220
Abell 1926N	0.136	14.0	940	1921	
Abell 2246	0.229	14.5	1300	491	HS1700+6416
MaxBCG J217.84740+24.68382[c]	0.097	13.9	1240	156	2MASS J1431258+244220
GMBCG J255.34805+64.23661	0.452	14.7	1400	1132	HS1700+6416

[a] Adopted cluster redshifts based on spectroscopic redshifts of BCGs.
[b] Impact parameter defined as projected distance between QSO sightline and X-ray centroid assuming Hubble flow distance at redshift of BCG.
[c] Values for r_{200} and M_{200} extracted from optical catalog (Rykoff et al. 2014)

Table 2. Summary of QSO observations

QSO	RA (J2000)	Dec (J2000)	z_{QSO}	T_{exp}	Instrument/Grating	Dataset IDs
SDSS J104741.75+151332.2	10 47 41.751	+15 13 32.30	0.4069	24881.2	COS G130M	LC8901010,LC8901020,LCKU09010
				18819.4	COS G160M	LCKU10010,LCKU11010
2MASS J1431258+244220	14 31 25.880	+24 42 20.68	0.3858	14523.9	COS G130M	LC8903010,LC8903020 LBS314010,LBS314020
HS1700+6416	17 01 00.620	+64 12 09.04	2.7407	175443.7	COS G130M	LC8301010-LC8312010
				101968.0	STIS E140M	O4SI02010-O4SI050A0

Пример квазарного спектра; рядом с лучом зрения есть 2 галактики скопления

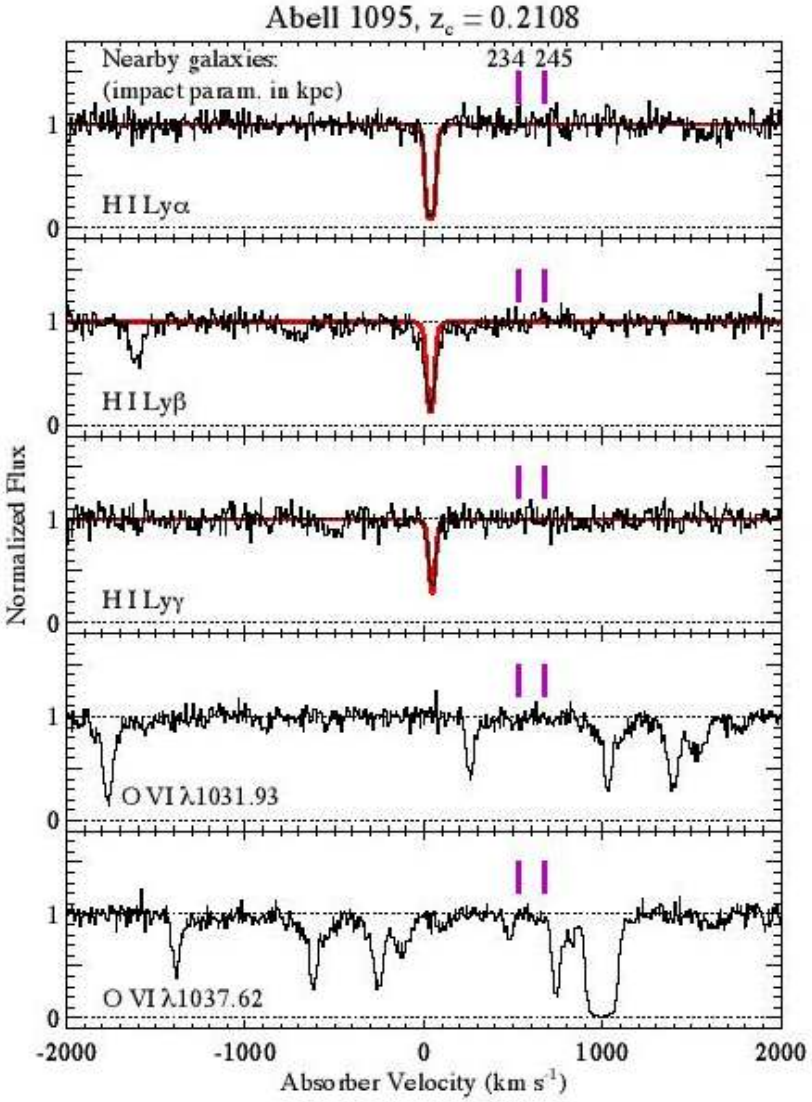

Результаты поиска линий водорода и OVI на красном смещении галактик

Cluster	z_{gal}	ρ [kpc]	log N(H I) [cm^{-2}]	log N(O VI)
MaxBCG J217.55+24.68	0.0939	269	<12.97	-
MaxBCG J217.55+24.68	0.0960	129	<12.90	-
MaxBCG J217.55+24.68	0.0993	193	<12.91	-
MaxBCG J217.55+24.68	0.0964	117	<12.91	-
MaxBCG J217.55+24.68	0.0961	236	<12.92	-
MaxBCG J217.55+24.68	0.0960	131	<12.92	-
MaxBCG J217.55+24.68	0.0963	210	12.97 ± 0.54	-
A1095	0.2130	234	<13.53	<13.11
A1095	0.2135	245	<13.54	<13.12
A2246	0.2285	44	<14.20[1]	<13.80
GMBCG J255.55+64.23	0.4560	73	<14.33	<14.62

[1] Upper limit includes the column density of unambiguously detected H I and any possible contribution of H I to nearby blended absorption features

Результаты

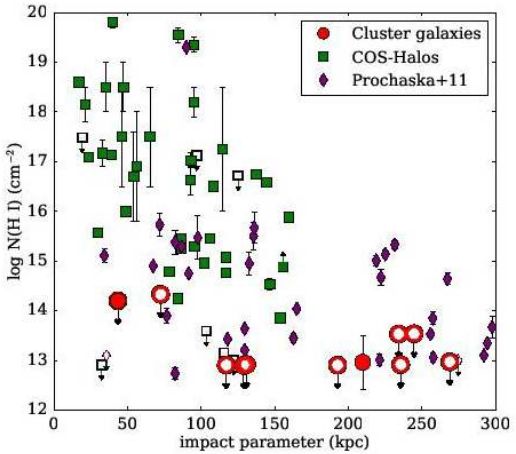

Figure 8. The H I column densities measured in our cluster galaxies' CGM compared with field galaxy CGM measurements from the literature. The red circles denote cluster galaxies from our sample, while the green and purple points correspond to CGM measurements of field galaxies. All upper limits (open symbols)

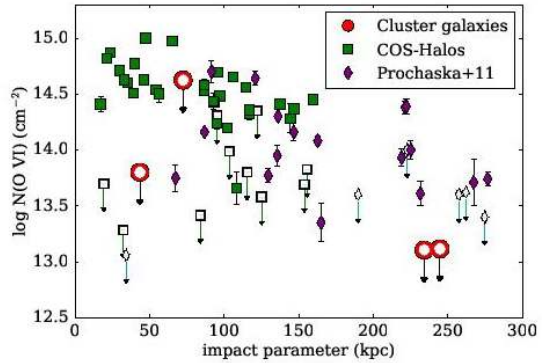

Figure 9. The O VI column densities measured in our cluster galaxies' CGM compared with field galaxy CGM measurements from the literature. The red circles denote cluster galaxies from our sample, while the green and purple points correspond to CGM measurements of field galaxies. All upper limits (open symbols) are 3σ. The column densities and galaxy information for our cluster galaxy sample may be found in Table 5.

- Для водорода
- Для OVI

И нейтрального водорода, и теплого газа меньше, чем у галактик поля

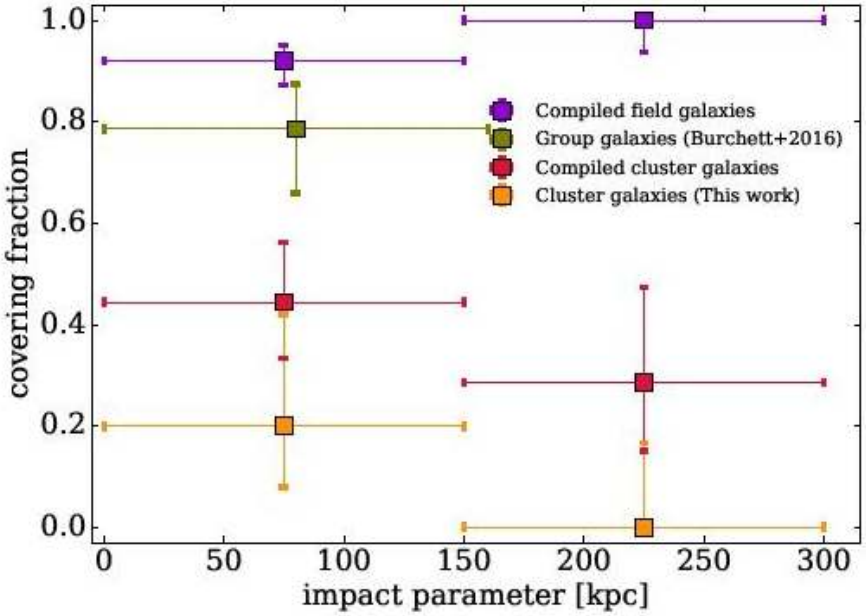

Figure 12. Covering fractions of H I in the CGM, calculated in bins of impact parameter indicated by the horizontal lines, of galaxies across various environments. Shown are a field galaxy sample (purple) combining those of Tumlinson et al. (2013), and Prochaska et al. (2011), galaxies in group environments (green) from Burchett et al. (2016), a cluster sample (red) combining this work and that of Yoon & Putman (2013), and the data from this work alone (orange). For comparison, we have imposed the same 100 mÅ detection threshold as Yoon & Putman (2013) for our covering fraction measurement. The cluster galaxies show markedly lower covering fractions than those of field galaxies.